Supporting Information

Perovskite-coated small-size single-crystalline W-doped Ni-rich cathodes with greatly enhanced power density for Li-ion batteries

Hujun Zhang[a], Li Qin[a], Xing Huang[b], Yaoguo Fang[b], Haifeng Yu[a], Qilin Cheng[a]*, Hao Jiang[a]**

[a]*Key Laboratory for Ultrafine Materials of Ministry of Education, Shanghai Engineering Research Center of Hierarchical Nanomaterials, School of Materials Science and Engineering, East China University of Science and Technology, Shanghai 200237, China*

[b]*Shanghai Xuanyi New Energy Development Co., Ltd, Shanghai 201800, China*

E-mail address: y.fang2@gotion.com (Dr. Y. G. Fang), chengql@ecust.edu.cn (Prof. Q. L. Cheng), jianghao@ecust.edu.cn (Prof. H. Jiang)

*Corresponding authors.

Tel.: +86-21-64250949; Fax: +86-21-64250624.

Part I: Methods

1.1 Materials synthesis

The precursors were prepared by the co-precipitation method. First, a certain proportion of $NiSO_4 \cdot 6H_2O$, $CoSO_4 \cdot 7H_2O$, and $MnSO_4 \cdot H_2O$ was dissolved in a certain volume of deionized water to configure a 2 mol L^{-1} transition metal salt solution A. Meanwhile, a 3.0 mol L^{-1} $NH_3 \cdot H_2O$ solution was prepared as the complexing agent B, and a 4 mol L^{-1} NaOH aqueous solution as the precipitant C. Subsequently, solutions A, B, and C were simultaneously added at a certain rate to a 5 L co-precipitation reactor containing a certain concentration of ammonia and water mixture (1.0 mol L^{-1}), and the pH of the solutions was controlled to be first high and then low, the stirring rate was 800 r min^{-1}, the reaction temperature was 55 °C, and the reaction was carried out under the atmosphere of N_2/O_2 mixture. After reacting for 20 h and then aging for 6 h, $Ni_{0.85}Co_{0.05}Mn_{0.10}(OH)_2$ precursor powder was obtained by washing with deionized water, filtering and drying.

The synthesis of conventional particle size pure samples $LiNi_{0.85}Co_{0.05}Mn_{0.10}O_2$ (NCM), conventional size W-doped (W-NCM), small size W-doped (*s*-W-NCM), and small size W-doped synergistic La_4NiLiO_8-coated cathode (*s*-W-NCM@LNLO) were carried out by a short-time pulse high temperature sintering (PHTS) method. The $LiOH \cdot H_2O$ (5% excess) was firstly mixed with $Ni_{0.85}Co_{0.05}Mn_{0.10}(OH)_2$ ($TM(OH)_2$) precursors. Then, the mixture was sintered in O_2 atmosphere at a multiple-step temperature procedure: a preheating at 500 ℃ for 3 h in advance, then heating at 765 ℃ for 4 h, followed by a short-time PHTS process (1020 ℃ for 1 min), then cooling down to 765 ℃ and holding it for 4 h to obtain the single-crystalline NCM samples. Next, *s*-W-NCM and *s*-W-NCM@LNLO samples were synthesised using the same sintering process for NCM synthesis. It should be noted that the W source is added to the precursor as dry WO_3 with 0.3 mol%. The La sources were introduced by dispersing 2 wt% of $La(NO_3)_3 \cdot 6H_2O$ in 30 mL of anhydrous ethanol and stirring vigorously for 30 min to obtain a

homogeneous mixture. Subsequently, 1 g of the precursor was poured into the above mixture and stirred in a water bath at 100 °C until dry. Lastly, in order to investigate the effect of particle size on electrochemical properties. We introduced 0.3 mol% of WO_3 in dry form for milling and mixing with NCM after synthesising single-crystalline NCM. Then the W-NCM sample was synthesised by holding at 800 °C for 10 h.

1.2 Material characterization

The morphology and microstructure of the samples were characterized using field emission focused ion beam scanning transmission electron microscopy (SEM, Hitachi S-4800) and field emission transmission electron microscopy (TEM, Talos F200X). The inductively coupled plasma atomic emission spectrometer (ICP-AES, Agilent 725) was conducted for elemental analysis. The crystalline phases of the single-crystalline Ni-rich cathodes were investigated using an X-ray diffraction (XRD, Ultima IV) and crystallography data analysis software (GSAS) refinement. The surface chemistry before and after cathodic cycling was investigated using an X-ray photoelectron spectrometer (XPS, ESCALAB 250Xi), and the resulting data were calibrated using the C 1s peak (284.8 eV). The *in-situ* XRD measurements were performed within 2.7-4.3 V at 0.33C (1C = 180 mA g^{-1}) by Rigaku Ultima IV connecting with a Gamry electrochemical workstation.

1.3 Electrochemical test

All cathodes underwent testing for Coulombic efficiency, rate performance, and cycling performance in a CR2016 coin cell using a LAND battery tester (CT2001A, 1C = 180 mA g^{-1}). Cyclic voltammetry (CV) curves and electrochemical impedance spectroscopy (EIS) tests were conducted using a Metrohm electrochemical workstation (Autolab PGSTAT302N) at an experimental frequency of 100 kHz-0.01 Hz. The galvanostatic intermittent titration technique (GITT) test involved charging/discharging the battery at 0.1C for 20 min, followed by a 1 h rest at open circuit. To assemble the button cell, the positive active material (80 wt%) was mixed

with the conductive agent (Super-P, 10 wt%) and the binder polyvinylidene fluoride (PVDF, 10 wt%) through stirring, and then uniformly coated onto an aluminum foil using N-methyl-2-pyrrolidone (NMP) as a solvent. The positive electrode sheets were loaded with a mass of 1.7-2.5 mg cm^{-2}. The electrolyte used was 1.2 M $LiPF_6$ in ethylene carbonate (EC) and ethyl methyl carbonate (EMC) (volume ratio = 7:3) with 2 wt% vinylene carbonates (VC), and the cell separator was a polypropylene membrane (Celgard 2400). The assembly process was carried out in an argon glove box with H_2O and O_2 levels below 0.01 ppm. The rate performance and cycle performance tests of pouch batteries were conducted using the NEWARE battery tester (BTS4000). For the assembly of the pouch-type full-cells, the cathodic electrode consisted of active material, polyvinylidene fluoride (PVDF), conductive agent carbon black (Super-P), and carbon nanotubes (CNT) in a weight ratio of 94:3:1.5:1.5. The loading mass of cathodic electrode was 12 mg cm^{-2}. The commercial graphite was used as the anode (7.5 mg cm^{-2}). The N/P ratio was approximately 1.1. Then the cut cathode (4.1×6.3 cm^2), anode (4.3×6.5 cm^2) and diaphragm are stacked and wound into a square cell of Li-ion battery in sequence and welded with battery tab. Amounts of electrolyte used in coin cell and in pouch cell are 100 μL and 3 mL, respectively. Afterward, the aluminum-plastic film was thermally encapsulated into a square cell of Li-ion battery, and the electrolyte was injected into an argon-filled glove box after the process of resting, second sealing, formation, and capacitance fixing to obtain the 50 mAh pouch full-cells.

1.4 The testing process and calculation equation of GITT measurement

For the GITT measurement, the assembled coin-type half-cells were firstly galvanostatic charge/discharged at a constant current of 0.1C for 2 cycles. Subsequently, the charging/discharging interval was set as 20 min, and the open circuit lasted 1 h to allow the cell voltage to relax to its quasi-equilibrium state. The change in the steady-state voltage ΔE_s is obtained by subtracting the original voltage (E_0) from the steady-state voltage (E_s). The cell

voltage increases during the current flux and the total change of cell voltage ΔE_τ can be obtained by calculating the voltage drop. Meanwhile, the process of the chemical diffusion is assumed to obey Fick's second law of diffusion. With a series of simplifications, for sufficient time interval ($\tau << L^2/D_{Li^+}$), the equation of D_{Li^+} can be written as (Equation 1):

$$D_{Li+} = \frac{4}{\pi}\left(\frac{m_B V_m}{M_B A}\right)^2 \left(\frac{\Delta E_s}{\tau\left(\frac{dE_\tau}{\sqrt{\tau}}\right)}\right)^2 \left(\tau \ll \frac{L^2}{D_{Li+}}\right) \qquad (1)$$

where V_m is the molar volume of active materials, M_B and m_B are the molecular weight and mass of the host oxide, respectively, and A is the total contact area between the electrolyte and the electrode, L is the thickness of the electrode. If sufficiently small currents and short time intervals are employed, the cell voltage is a linear function of the square root of τ, Equation 1 can be further simplified as (Equation 2):

$$D_{Li+} = \frac{4L^2}{\pi\tau}\left(\frac{\Delta E_s}{\Delta E_\tau}\right)^2 \left(\tau \ll \frac{L^2}{D_{Li+}}\right) \qquad (2)$$

where ΔE_s is the value of subtracting the original voltage (E_0) from the steady-state voltage (E_s). ΔE_τ is the change in the total temporary potential during the application of current in τ, L is the thickness of the electrode.[1-6]

Part II: Supporting Figures

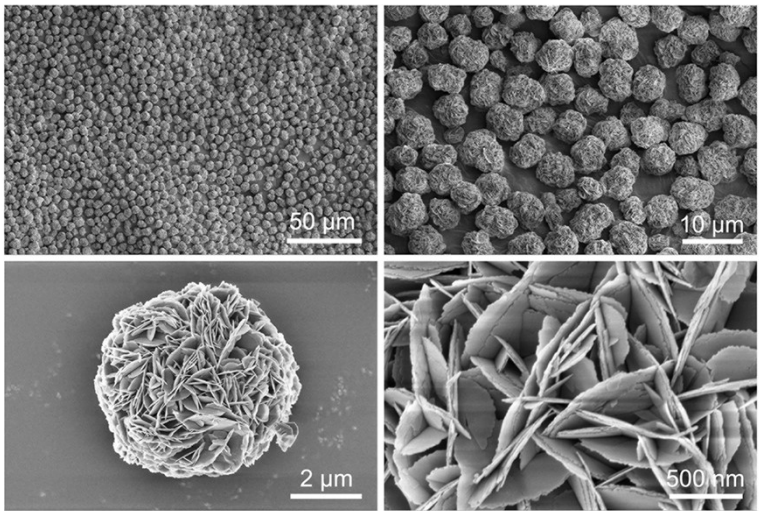

Fig. S1. SEM images of the $Ni_{0.85}Co_{0.05}Mn_{0.10}(OH)_2$ precursors.

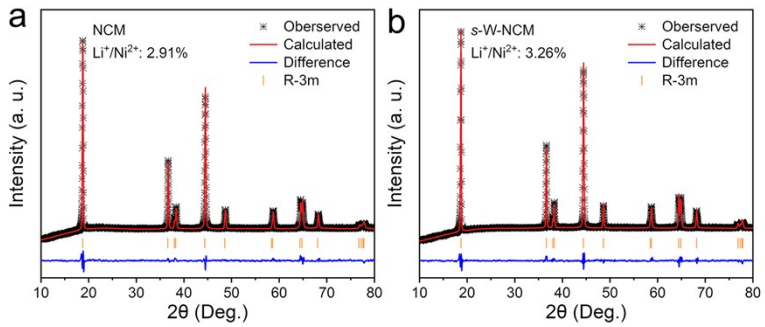

Fig. S2. XRD Rietveld refinements for (a) NCM and (b) *s*-W-NCM.

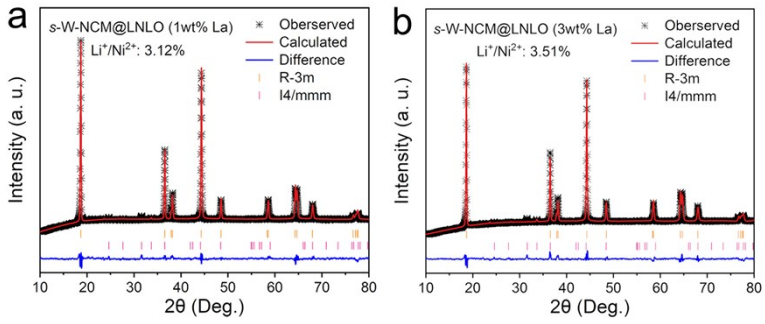

Fig. S3. XRD Rietveld refinements for (a) *s*-W-NCM@LNLO (1wt% La) and (b) *s*-W-NCM@LNLO (3wt% La).

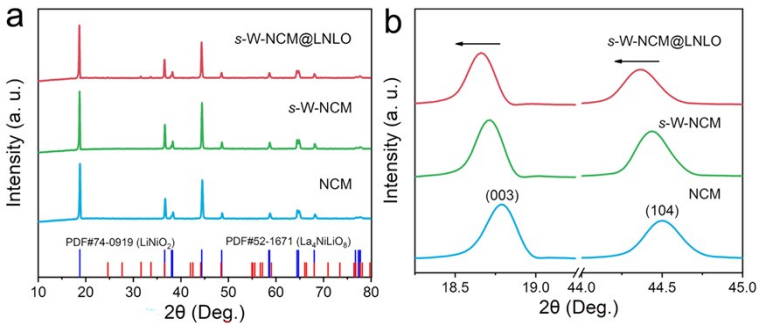

Fig. S4. (a) XRD patterns of pristine NCM, *s*-W-NCM, and *s*-W-NCM@LNLO (b) with the magnification region of (003) and (104) peaks.

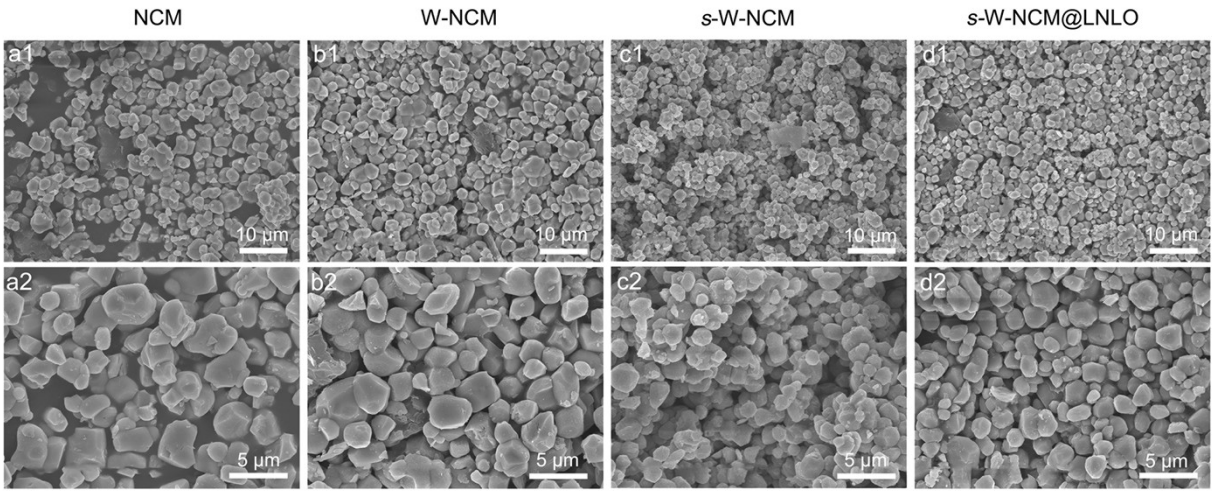

Fig. S5. SEM images of (a1, a2) NCM, (b1, b2) W-NCM, (c1, c2) *s*-W-NCM, and (d1, d2) *s*-W-NCM@LNLO.

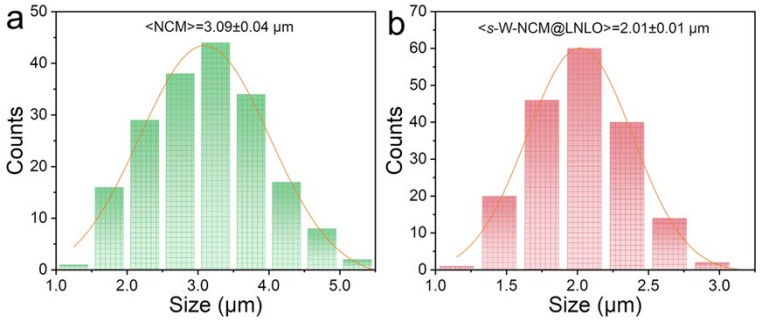

Fig. S6. Statistical plot of mean particle size distribution of (a) NCM and (b) *s*-W-MCM@LNLO.

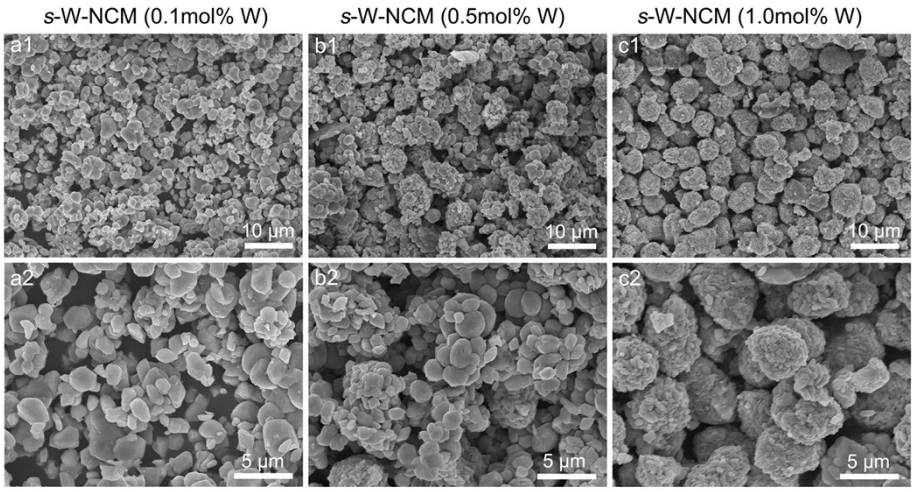

Fig. S7. SEM images of (a1, a2) *s*-W-NCM (0.1mol% W), (b1, b2) *s*-W-NCM (0.5mol% W), and (c1, c2) *s*-W-NCM (1.0mol% W).

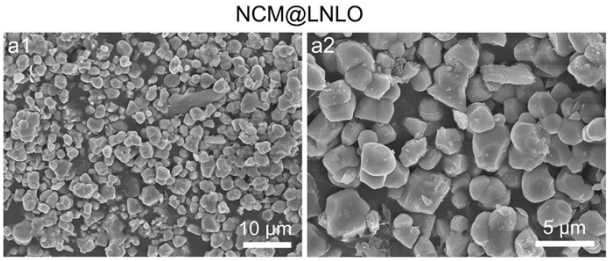

Fig. S8. SEM images of (a1, a2) NCM@LNLO.

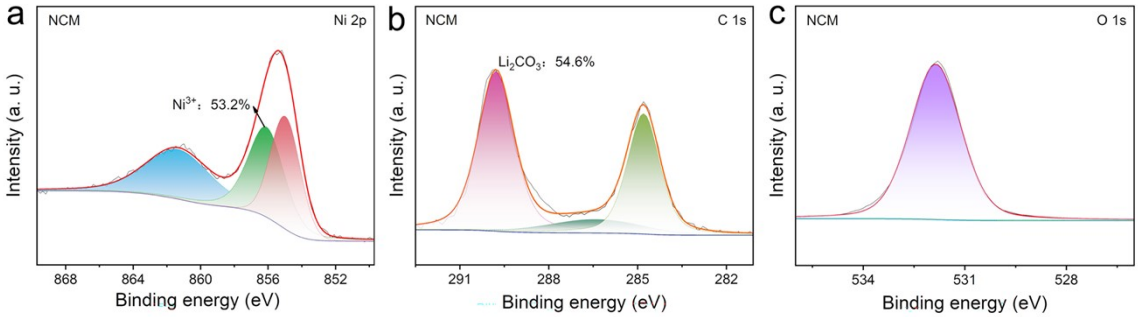

Fig. S9. (a) Ni 2p, (b) C 1s and (c) O 1s XPS spectra of NCM.

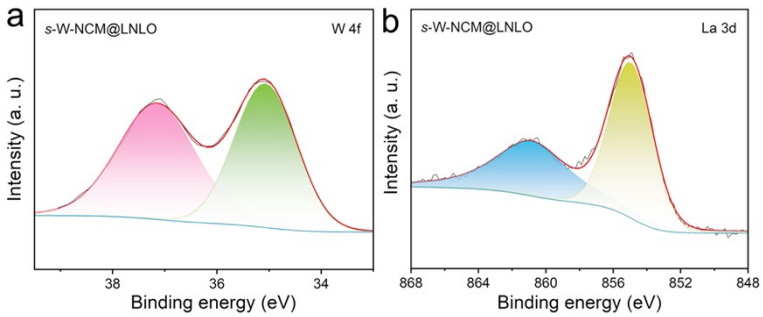

Fig. S10. (a) W 4f and (b) La 3d XPS spectra of *s*-W-NCM@LNLO.

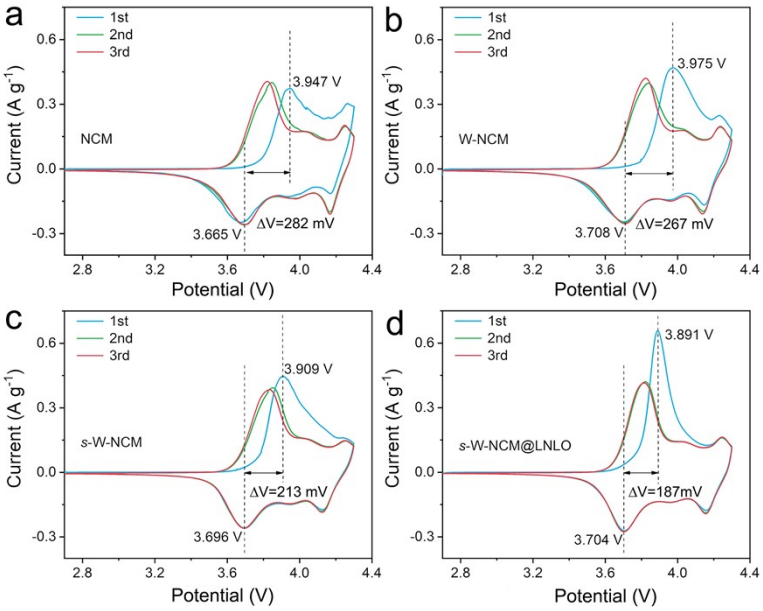

Fig. S11. The initial three CV curves of (a) NCM, (b) W-NCM, (c) *s*-W-NCM, and (d) *s*-W-NCM@LNLO at 0.1 mV s^{-1}.

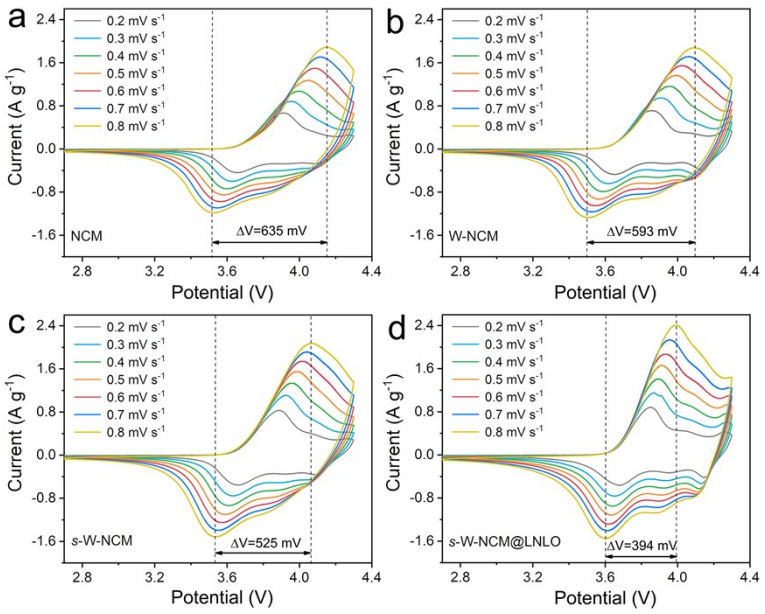

Fig. S12. CV curves of (a) NCM, (b) W-NCM, (c) *s*-W-NCM, and (d) *s*-W-NCM@LNLO from 0.2 to 0.8 mV s^{-1}.

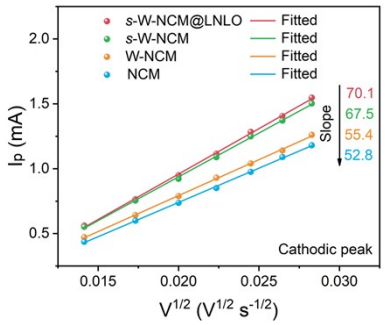

Fig. S13. Linear relationship between the cathodic peak current (i_p) and the square root of the scan rate ($v^{1/2}$) for NCM, W-NCM, *s*-W-NCM, and *s*-W-NCM@LNLO.

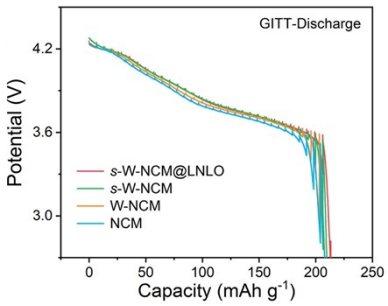

Fig. S14. GITT curves during discharging of NCM, W-NCM, *s*-W-NCM, and *s*-W-NCM@LNLO.

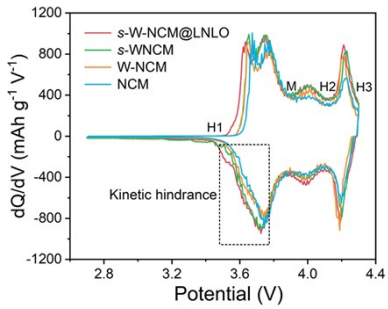

Fig. S15. dQ dV^{-1} profiles obtained by differentiating charge-discharge curves at 0.1C of NCM, W-NCM, *s*-W-NCM, and *s*-W-NCM@LNLO.

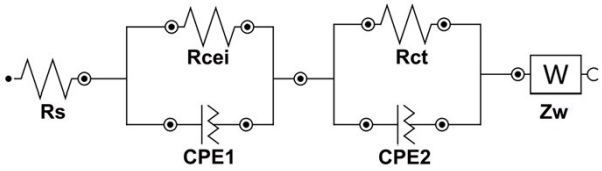

Fig. S16. The equivalent fitting circuit diagram for EIS testing.

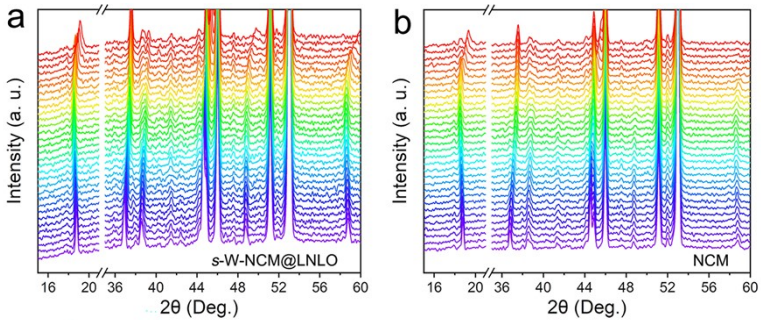

Fig. S17. The all diffraction peaks at electrochemical *in-situ* XRD patterns of the (a) NCM and (b) *s*-W-NCM@LNLO.

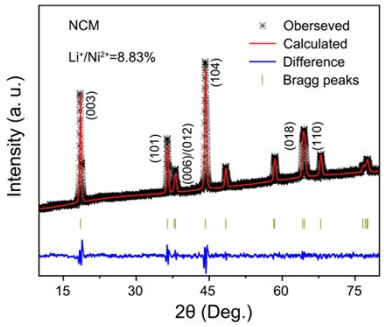

Fig. S18. XRD Rietveld refinement of NCM after 200 cycles at 1C.

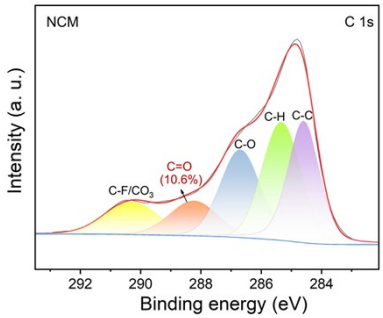

Fig. S19. C1s XPS spectra of NCM after 200 cycles at 1C.

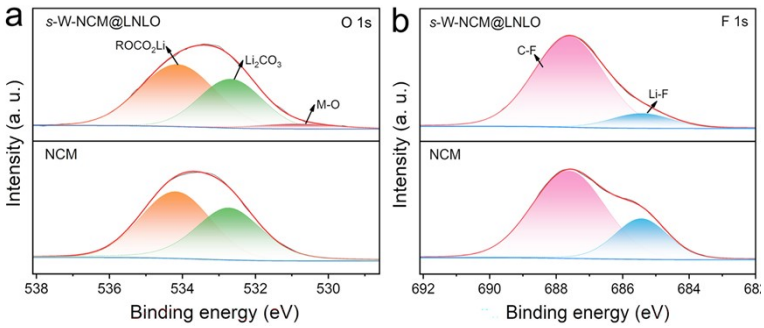

Fig. S20. (a) O 1s and (b) F 1s XPS spectra of NCM and *s*-W-NCM@LNLO after 200 cycles at 1C.

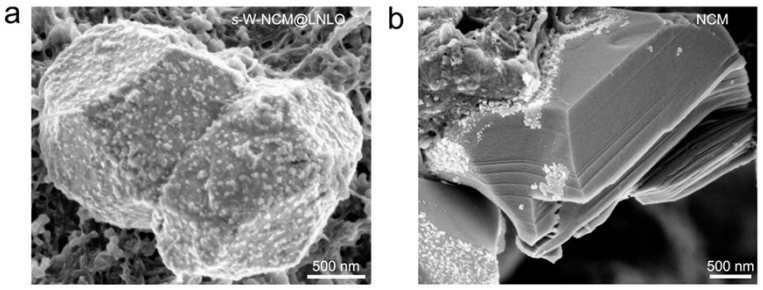

Fig. S21. SEM images of (a) NCM and (b) *s*-W-NCM@LNLO after 200 cycles at 1C.

Part III: Supporting Tables

Table S1. Lattice parameters of the NCM, W-NCM, *s*-W-NCM, and *s*-W-NCM@LNLO cathodes calculated from XRD Rietveld refinement.

Samples	Lattice parameters				Li^+/Ni^{2+}	wR_p	χ^2
	a(Å)	c(Å)	c/a	V(Å^3)			
NCM	2.8805	14.2294	4.940	102.249	2.91%	2.39%	0.679
W-NCM	2.8729	14.1899	4.939	101.425	3.04%	2.05%	0.544
***s*-W-NCM**	2.8746	14.2059	4.942	101.651	3.26%	2.39%	0.691
***s*-W-NCM@LNLO**	2.8781	14.2151	4.939	101.979	2.76%	2.25%	0.611
***s*-W-NCM@LNLO1**	2.8748	14.2040	4.941	101.526	3.12%	2.45%	0.720
***s*-W-NCM@LNLO3**	2.8704	14.1836	4.941	101.208	3.51%	2.69%	0.809

Table S2. Chemical compositions for the NCM, W-NCM, *s*-W-NCM, and *s*-W-NCM@LNLO measured by ICP-AES.

Samples	Mole ratio					
	Li	Ni	Co	Mn	W	La
NCM	0.9991	0.8491	0.0510	0.0999	/	/
W-NCM	1.0023	0.8472	0.0481	0.1019	0.0028	/
s-W-NCM	1.0045	0.8481	0.0487	0.1006	0.0026	/
s-W-NCM@LNLO	1.0012	0.8364	0.0472	0.0965	0.0027	0.0041

Table S3. Comparative tables of rate performance of reported single-crystalline Ni-rich cathodes and *s*-W-NCM@LNLO for high-energy-density lithium-ion batteries.

Samples	Average Size	Discharge Rate	Voltage Range	Capacity (mAh g^{-1})	References
s-W-NCM@LNLO	~ 2 μm	1C/5C/10C	2.7-4.3 V	183.9/136.8/111.8	This Work
MSC-NCM9055	~ 1.3 μm	5C/10C	2.7-4.3 V	128.7/101.9	[7]
SC-NCMA@LAP	2-4 μm	5C	2.7-4.3 V	112.8	[8]
SC-NCM811@LLAO	2-4 μm	5C	2.8-4.3 V	127.8	[9]
SC-NCM9055	~ 2 μm	1C	2.7-4.3 V	179.2	[10]

Table S4. Lattice parameters of the NCM and *s*-NCM@LNLO cathodes calculated from XRD Rietveld refinement after 200 cycles.

Samples	Lattice parameters				Li^+/Ni^{2+}	wR_p	χ^2
	a(Å)	c(Å)	c/a	V(Å^3)			
NCM	2.8936	14.2472	4.924	102.621	8.83%	3.85%	0.667
***s*-W-NCM@LNLO**	2.8823	14.2291	4.937	102.038	6.05%	3.49%	0.447

References

[1] H. Yu, Y. Cao, L. Chen, Y. Hu, X. Duan, S. Dai, C. Li and H. Jiang, *Nat. Commun.*, 2021, **12**, 4564.

[2] H. Yu, H. Zhu, H. Jiang, X. Su, Y. Hu, H. Jiang and C. Li, *Natl. Sci. Rev.*, 2023, **10**, nwac166.

[3] H. Zhu, Z. Wang, L. Chen, Y. Hu, H. Jiang and C. Li, *Adv. Mater.*, 2023, **35**, 2209357.

[4] Z. Wang, W. Wei, Q. Han, H. Zhu, L. Chen, Y. Hu, H. Jiang and C. Li, *ACS Nano*, 2023, **17**, 17095-17104.

[5] Q. Han, H. Yu, L. Cai, L. Chen, C. Li and H. Jiang, *Proc. Natl. Acad. Sci. U.S.A.*, 2024, **121**, e2317282121.

[6] H. Zhang, L. Qin, M. Sedlacik, P. Saha, Q. Cheng, H. Yu and H. Jiang, *J. Mater. Chem. A*, 2024, **12**, 3682-3688.

[7] H. Huang, H. Zhu, J. Gao, J. Wang, M. Shao and W. Zhou, *Angew. Chem. Int. Ed.*, 2024, **63**, e202314457.

[8] H. Bai, K. Yuan, C. Zhang, W. Zhang, X. Tang, S. Jiang, T. Jin, Y. Ma, L. Kou, C. Shen and K. Xie, *Energy Storage Mater.*, 2023, **61**, 102879.

[9] Y. Liu, T. Zeng , G. Li , T. Wan , M. Li , X. Zhang , M. Li , M. Su , A. Dou , W. Zeng , Y. Zhou , R. Guo and D. Chu, *Energy Storage Mater.*, 2022, **52**, 534-546.

[10] H. Huang, L. Zhang, H. Tian, J. Yan, J. Tong, X. Liu, H. Zhang, H. Huang, S.-M. Hao, J. Gao, L. Yu, H. Li, J. Qiu and W. Zhou, *Adv. Energy Mater.*, 2023, **13**, 2203188.